Hydrothermally grown ZnO nanorods in different aspect ratios and their gas sensing properties

S. K. Jubear[a], O. M. Abdulmunem[b,*], E. S. Hassan[b]
[a]*Ministery of Education, Directorate General for Education, Baghdad, Iraq*
[b]*Physics department, college of science, Mustansiriyah University, Baghdad, Iraq*

On a glass substrate, zinc oxide nanorods (ZnO NRs) arrays of varying aspect ratios have been grown by hydrothermal method at 90 ^{O}C with variable ZnO seed layer thicknesses applied by RF sputtering. The structural properties and gas sensitivity of zinc oxide nanorods were studied by using X-ray diffraction (XRD) for analyzing the structural characteristics was discovered that ZnO NRs and seed layer films are both polycrystalline, with the same plane preferred reflection for (002). The seed layer's crystallite size ranges from 19.51 nm to 30.45 nm for thicknesses t_1 and t_4, respectively. The measurements of the FESEM showed aspect ratios for ZnO NRs ranging from 3.03 for t_1 to 4.9 for t_4, with growth in different shapes: ZnO NRs for t_1, flowers and rod-like shapes for thicknesses t_2 and t_3, and hexagonal-rod-like shapes for t_4. ZnO NRs based on gas sensors and tests of the response of prepared samples on NH_3 and CO_2 gases showed good sensitivity to both gases at different concentrations (1000, 2000, and 3000 ppm), reaching 65–70 at operating 50 ^{O}C.

(Received October 8, 2023; Accepted January 10, 2024)

Keywords: Zinc oxide nanorod, Hydrothermal method, Seed layer films, Gas sensing, Polycrystalline, RF sputtering

1. Introduction

In common uses and industrial production, most gases are colorless and tasteless. Incidents involving exposure to gases have occurred in laboratories, factories, companies, and private residences. Since human senses cannot distinguish several poisonous or harmful gases, gas sensors are required to detect the presence of potentially dangerous gases [1, 2]. The most prevalent gases of relevance include NO, CO, NH_4, NO_2, CO_2, SO_2, and CH_4, in addition to several volatile organic compounds, like acetone, benzene, ethanol, toluene, and methanol [3]. Because of their corrosivity, toxicity, or harmful effects, certain gases are dangerous even in parts per million (ppm) concentrations [4]. Gas sensors can be fabricated at both bulk and nano semiconductor scales. Bulk materials have shown deficient performance due to limited surface area [5]; in contrast, materials in the nanometer dimensions have exhibited superior performance due to their extreme surface area [6, 7]. Semiconducting metal oxides (SMOs) are the most often used materials in the production of gas sensors because they are straightforward and versatile [8]. More particularly, due to its high electron mobility and adaptability, ZnO has shown the most promise as a material for gas sensing [9]. ZnO can be defined as one of the suitable materials for a range of medical device applications since it is inexpensive, non-toxic, chemically stable, and biocompatible [10, 11].

1D ZnO nanostructures have been widely used as gas sensor materials thanks to the latest advancements in their synthesis. For this, many nanoscale geometries are being tested. Before now, ZnO nanomaterials were researched for use in gas sensors [12]. Since ZnO grows under conditions, it has unique nanostructures and is more diverse compared to other metal oxides in terms of all materials [13]. 1D ZnO nanostructures, such as nanowires, nanorods, and nanotubes, could provide more efficient carrier transport because they have fewer grain boundaries, surface defects, disorders, and discontinuous interfaces [14]. The efficiency of several ZnO nanostructure synthesis methods, such as hydrothermal synthesis, thermal evaporation, pulsed laser deposition, sputtering, and molecular beam epitaxy, have been put to comparison in earlier works [15]. Those growth processes,

* Corresponding author: munem@uomustansiriyah.edu.iq
https://doi.org/10.15251/DJNB.2024.191. 97

on the other hand, call for either pricey machinery, high vacuums, or high working temperatures, which could limit their potential applications, especially those requiring large-scale manufacture. The solution approaches, on the other hand, are scalable because of their low growing temperature, ease of manipulation, and low costs. The hydrothermal method of ZNR growth was studied in several studies, and it has proven to be flexible for synthesizing ZnO NRs. Sonalika Agarwal et al. [16] assessed two types of hydrothermally produced ZnO nanostructures, flower-like forms, and NRs, to investigate morphology-dependent gas sensing characteristics. In contrast to other invasive species evaluated, which responded poorly to ethanol or did not respond at all to carbon monoxide at ppm level, the two of such nanostructures' morphologies proved good sensitivity to NO_2 at ppb level. Yang, Daejeong, et al. [17]. The fabrication of ZnO nanorod gas sensor using a wet chemical process (a hydrothermal step and chemical bath deposition), photolithography, and lift-off procedures was effective and allowed for the low-power detection of a small amount of volatile organic compounds (VOCs). Through detecting Zinc hydroxy stannate (ZHS micro cubes/ZnO nanorods) nanocomposites, showing improved responsiveness to carbon oxide gas, Feng-Ren et al. [18] achieved a high surface-to-volume ratio, CO_2. This study aimed to enhance Zinc oxide nanorods to perform superior in detectors and sensors as NH_3 and CO_2 gases.

2. Experimental

ZnO NRs prepared hydrothermally on a glass substrate/ZnO seed layer of varying thickness (1135, 1306, 1437, 1533 nm), denoted by (t_1, t_2, t_3, and t_4), respectively, were deposited by RF-magnetron sputtering. The growth solution has been prepared by adding 1 mL of ammonia (Thomas Baker 29% NH_3) to 80 mL of deionized water (BI Supply deionized water) for obtaining a pH of 11 as measured by an LCD digital pH meter, with an accuracy of 0.01, operating temperature of 90 ^{O}C. 0.6663 g of zinc nitrate [ZnO $(NO_3)_2$. $6H_2O$] (PIOCHEM Molar mass = 297.47 g/mol) of 99.99 purity weight was measured through electrical balance sensitive to 4 digits (10-4 gm) was found by Eq. (1) [19]:

$$M = \frac{m}{M.wt} \times \frac{1000}{V} \quad (1)$$

where M is the concentration of molarities, m is the mass of zinc nitrate [$ZN(NO_3)_2 \cdot 6H_2O$], M_{wt} is the molecular weight regarding zinc nitrate [$ZN(NO_3)_2 \cdot 6H_2O$], volume regarding the deionized water (80 ml).

The gas sensitivity was measured using a setup that included an evaporation flask and a heating trough for evaporating the reactive compounds. The concentration of the gas entering the measuring chamber is found by Eq. (2). The measurement chamber was attached to a custom-made, vacuum-tight stainless steel cylindrical test chamber 20 cm in diameter and 16 cm in height, filled with ammonia gas using a needle valve. The base is detachable and has an O-ring to seal it. The chamber has an effective capacity of 5024 cm3, and it was evacuated to a pressure of 1×10^{-3} mTorr using a dry rotary pump (P101195 - Alcatel 2010 Pascal dual-stage rotary).

In Figure 1, the process of dissolving and homogenizing the growth solution was performed for 15 min by a magnetic stirrer at room temperature (25–30 ^{O}C); the zinc oxide seed layers have been after that fixed in a Teflon holder horizontally with the ZnO seed layer facing down, ensuring that all the samples have been immersed in the growth solution. The Teflon cell was transferred to the stainless-steel autoclave (200 mL capacity) and was closed tightly to place in an oven (Thermoline: Toh-150f) at 90 ^{O}C for three hours. The samples were left to cool naturally, and the forms were rinsed with deionized water.

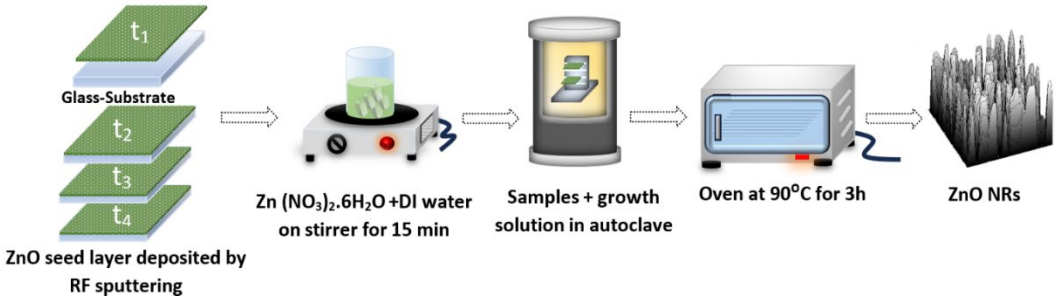

Fig. 1. Illustrated the process steps for growing ZnO NRs by the hydrothermal method.

The gas sensitivity was measured using a setup comprising an evaporation flask and a heating trough to allow the reactive chemicals to evaporate. The mask was made for gas sensing measurements with dimensions from aluminum foil sheets to obtain the desired shape of the electrodes. A thin coating of aluminum as electrodes has been deposited to ZnO NRs films using a thermal evaporation technique (Edward type).

A needle valve was used to introduce the ammonia gas into the measurement chamber, which was connected to a specially made, stainless steel cylindrical test chamber 16 cm in height and 20 cm in diameter. The base is removable and is sealed with an O-ring. The chamber's effective capacity is 5024 cm^3, and it was evacuated with a dry rotary pump (P101195 - Alcatel 2010 Pascal dual-stage rotary) to a pressure of 1×10^{-3} mTorr. Eq. (2) determines the NH_3 and CO_2 gases concentration of the gas entering the measuring chamber [20].

$$\frac{(V_d)\text{Volume of target gas(Ml)}}{V_c\text{Volume of test chamber(Ml)}} = \frac{\text{Volume(ppm)}}{10^6} \tag{2}$$

3. Results and discussion

3.1. Structural properties

Figure (2) illustrates the XRD pattern of ZnO NRs growth on glass/ZnO seed layers with various thicknesses (1135, 1306, 1437, 1533 nm) by a hydrothermal method. The diffraction pattern for all models is polycrystalline with a wurtzite ZnO structure according to the JCPDS 36-1451 card; the dominant reflection is the (002) plane at angle 2θ = 34.42° for all samples. The increase in the crystallite size of the (002) reflection with increasing seed layer thickness is indicated in Table (1).

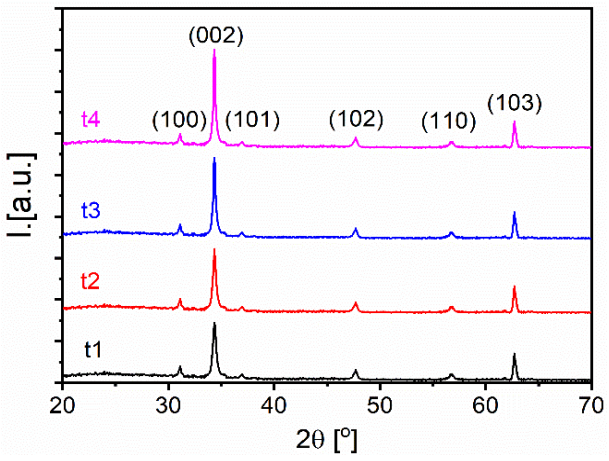

Fig. 2. XRD pattern of ZnO NRs synthesized by hydrothermal method.

Table 1. XRD result and structural parameters for ZnO NRs growth by hydrothermal method.

Sa.	2θ [°]	(hkl)	lattice constant [Å]				Crystallite size [nm]	Macrostrain $\times 10^{-5}$	Dislocation density $\times 10^{-5}$ [1/m^{-2}]
			Observed		JCPDS				
			a	c	a	c			
t_1	34.5	(002)	3.251	5.231	3.249	5.206	31.86	11.37	9.84
t_2	34.5	(002)	3.251	5.231	3.249	5.206	32.46	11.161	9.49
t_3	34.5	(002)	3.251	5.231	3.249	5.206	34.65	10.45	8.32
t_4	34.5	(002)	3.251	5.231	3.249	5.206	37.82	9.57	6.98

Figure (3) shows the typical FESEM images regarding ZnO NRs, prepared by hydrothermal method on a glass/ZnO seed layer deposited by the RF magnetron sputtering method. Figure (4a) represents t_1 with a seed layer thickness of 1135 nm and a seed layer average particle size of 20.23 nm. It is evident from the FESEM images that the growth of nanostructures was rod-like, dense, and perpendicular to the substrate surface, with diameter ranges of 27-152 nm, length ranges of 187-628nm, and an aspect ratio of 3.04. Figure (3b) is t_2 with a seed layer thickness of 1306 nm and an average seed layer particle size of 20.82 nm. The rods aggregated to form bundles of ZnO NRs parallel and vertical to the substrate surface with high density and irregular hexagonal shapes, a length range of 500–754 nm, a diameter range of 80–120 nm, and an aspect ratio of 4.11. Figure (3c) represents t_3 with a seed layer thickness of 1,437 nm and an average seed layer particle size of 26.09 nm. The bundle shapes in t_2 turned into irregular hexagonal ZnO NRs with a diameter range of 35–70 nm, length range of 200–426 nm, and aspect ratio of (3.9). Figure (3d) represents t_4 with a seed layer thickness of 1533 nm and an average seed layer particle size of 26.98 nm.

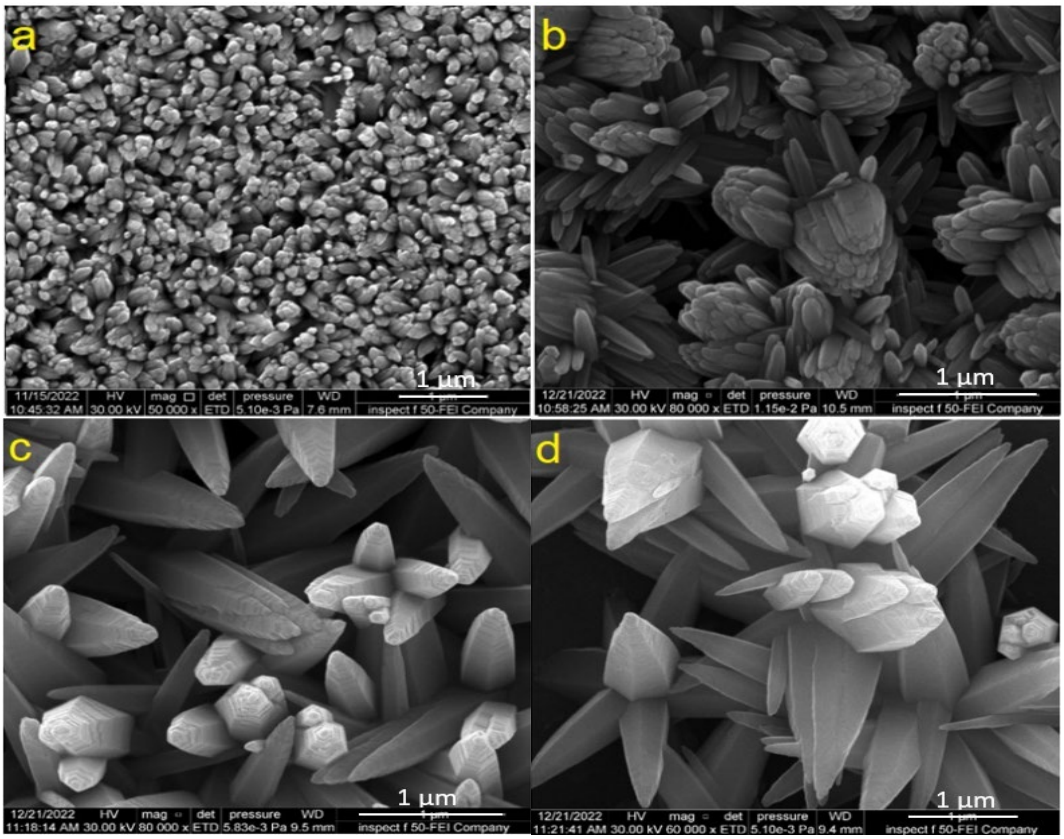

Fig. 3. FESEM images for ZnO NRs growth by hydrothermal method(a)t_1, (b)t_2, (c)t_3 and (d)t_4.

The growth showed a homogeneous distribution, good alignment, and uniform perpendicular growth on the substrate surface, with an average diameter of 117 nm, average length of 628 nm, and aspect ratio of 4.9. From the previous calculations length and diameter of the rods growing on the ZnO seed layers compared with their thickness, the aspect ratio increases with increasing thickness. This ratio skyrocketed to 4.9 at t_4, creating a substantial surface area that proves advantageous for various applications, including gas sensors [21].

3.2. Gas sensor properties

The oxidizing CO_2 and the reducing NH_3 gases have been used to study and test the ZnO NRs' gas-sensing capabilities. The adsorption-absorption gas sensing mechanism as well as the change in current, are the sensing signals in the case when a sensing element is made with the use of SMO such as ZnO [22]. In Figure (4), the oxygen atoms at the surface adsorbed related to ZnO NR material in air, and electrons from (O^{-2}, O^{-}, and O^{-2}) are collected to transform into surface acceptor states. On ZnO NRs surface, an electron depletion region with a high potential barrier is created because of the conduction band's electron loss and making it difficult for electrons to flow between the crystal grains [23, 24]. The semiconductor material's surface resistance fluctuates and approaches equilibrium.

Fig. 4. Sensing mechanism (adsorption, absorption of oxide and reduced gas) of ZnO NRs.

As shown in Figure (4), in the case when the samples are exposed to NH_3 gas molecules, the gas molecules react with oxygen ions (O^{-2}, O^{-}, O^{-2}) that are absorbed on the ZnO surface and then allow the electrons to return to the conduction band. This increases the carrier concentration and thins the depletion layer, which results in a reduction in resistance. When ZnO films are exposed to a reducing gas, like NH_3, the resistance decreases; this shows that ZnO is an n-type semiconductor [25]. The reactions of this process can be described using Equation (1) [26].

$$2NH_3 + 3O_{2-(ads)} \rightarrow N_2 + 3H_2O + 3e^- \quad (1)$$

Figure (5) denotes the resistance curve as a function of time and illustrates the sample behavior during exposure to NH_3. Where t_1 decreases in resistance at the gas concentration of 1000 ppm to reach 10 MΩ with decreases in resistance for 2000 ppm and 3000 ppm to reach 8 MΩ, besides other samples following the same behavior. However, t_4 showed a lower resistance when exposed to the target gas than the other models, reaching 5 MΩ with a gas concentration of 3000 ppm due to the higher aspect ratio for this sample of 4.9 which leads to increased reactions between ZnO NRs and the gas molecules [27].

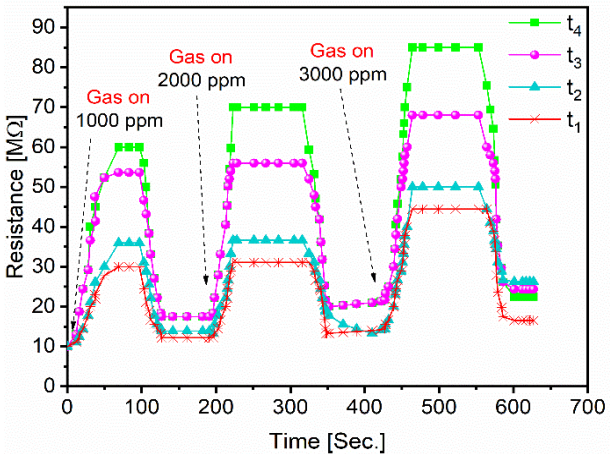

Fig. 5. Change in resistance as function of time for ZnO NRs growth by hydrothermal exposure to varies concentrations of NH_3 gas.

The sensitivity of the ZnO NRs to the gas was calculated using Eq. (3) [28] for t_1, t_2, t_3, and t_4, as shown in Figure (5).

$$S = \left|\frac{Ra-Rg}{Ra}\right| \times 100\% \quad (3)$$

where *Rg* and *Ra* stand for the sensor's gas resistance and air resistance, respectively.

Target gas concentration, temperature, and grain size of sensing material all have an impact on the sensitization procedure [29]. The electrical resistance of the ZnO NRs depends on the crystallite size and the distance of the depletion zone, which is sometimes also called the space charge layer (2L), and the conduction electrons should pass through such channels along with the grain boundary barrier [30]. Due to the high concentration of crystal grains in the material, multiple channels form, and the resistance of the channels influences the sensor's resistance [31]. The target gas concentration has an impact on sensitivity as well; when a small area of the sample is exposed to a low gas concentration, a smaller gas molecule coverage leads to a smaller surface response, which diminishes gas sensing. The surface response, on the other hand, raises for a greater surface coverage brought on by an increase in gas concentration, demonstrating superior gas sensing. In the case when the molecule coverage reaches its saturation point, further increases in surface reactions become gradual.

Thus, in this study, the sensitivity values were obtained for t_1, t_2, t_3, and t_4. Increases in the seed layer thickness led to increases in both the crystallite size and aspect ratio, thus an increase in sensitivity, which explains why t_4 showed the highest sensitivity among the other models.

The sensitivity of t_1, with an aspect ratio of 3.04 at 3000 ppm, was 44.57. It increased with an increasing aspect ratio to 4.9 with a sensitivity of 65 at t_4. As shown in Figure (6a), increases in the target gas concentration from 1000 to 3000 ppm NH_3 led to sensitivity increases for all the samples [32]. It was observed that the response time dropped from 70 s in t_1 to reach some of a second for t_4 at 3000 ppm, as shown in Figure (6b).

This was due to an increase in the number of reactions as a result of the large aspect ratio and gas concentration; the recovery time increased with the increase in both gas concentration and aspect ratio to reach almost 100 s, as shown in Figure (6c), due to saturation or an operating temperature effect on ZnO NR which changed its properties, as listed in Table 2.

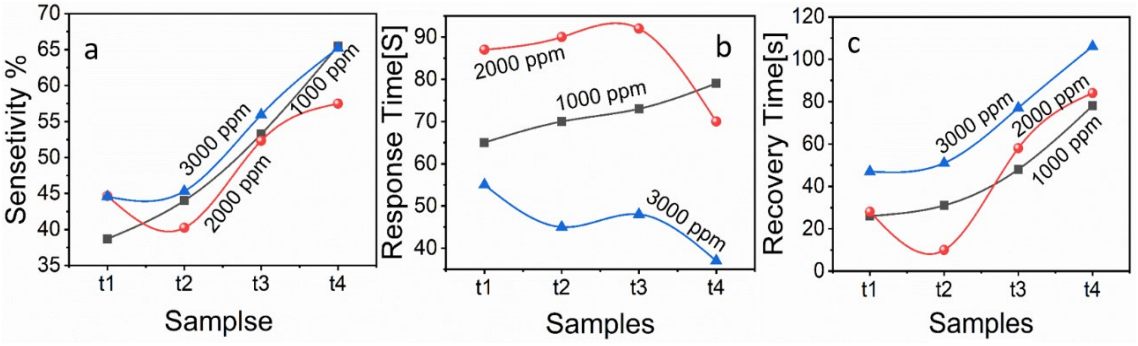

Fig. 6. ZnO NRs deposited on the glass substrate by RF sputtering for different NH_3 concentrations (a) Sensitivity, (b) Response time and (c) Recovery time.

Table 2. Results of sensing measurement of ZnO NRs to NH_3 gas.

Sa.	sensitivity			Response time (s)			Recovery time (s)		
	Gas concentration (ppm)			Gas concentration (ppm)			Gas concentration (ppm)		
	1000	2000	3000	1000	2000	3000	1000	2000	3000
t_1	38	44	44	65	87	55	26	28	47
t_2	44	40	45	70	90	45	31	10	51
t_3	53	52	55	73	92	48	48	58	77
t_4	65	57	65	70	70	37	78	84	106

As in the sensing mechanism, when CO_2 is exposed as an oxide gas, CO_2 gas molecules acquire electrons from ZnO NRs' conduction band as a result of interactions with adsorbed oxygen molecules, which create adsorbed $CO_2^-{}_{(ads)}$ [33]. As a result, following exposure to CO_2 gas, electron transfer occurs from ZnO to CO_2 gas molecules, increasing the electrical resistivity of the ZnO NRs sensor until the saturation point, at which point the resistance becomes constant. The following is a description of the reaction process [34, 35]:

$$CO_{2(gas)} + e^- \rightarrow CO^{-2}{}_{(ads)} \quad (2)$$

$$CO_{2\,(gas)} + O^-{}_{2(ads)} + 2e^- \rightarrow CO^{-2}{}_{(ads)} + 2O^-{}_{(ads)} \quad (3)$$

It was observed that the resistance of the sample significantly increased in the presence of CO_2 due to the absorption of oxygen ions on the surface of ZnO NRs [36]. Moreover, the system was almost restored to its initial state when the target gas was removed. Also, the surface resistance of t_1 increased when exposed to CO_2 to 30 MΩ, as shown in Figure (7). When the concentration of the gas increased, and resistance also increased due to an increase in the number of gas molecules absorbed on the surface of ZnO NRs, t_4 showed the highest resistance values for all gas concentrations of 95 MΩ in 3,000 ppm for high aspect ratios, as shown in Table 3.

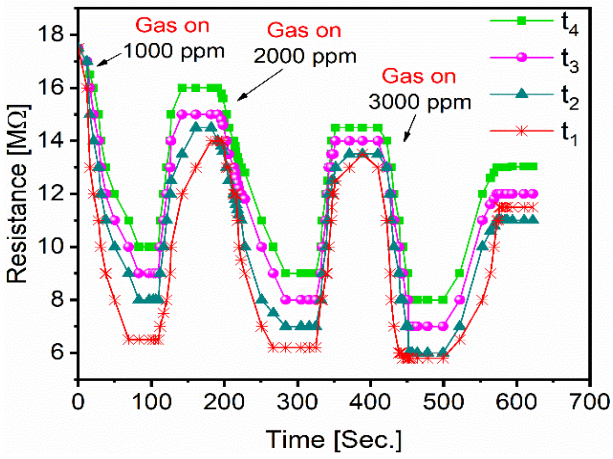

Fig. 7. Shows the change in resistance as function of time for ZnO NRs growth by hydrothermal exposure to varies concentrations of CO_2 gas.

Table 3. Results of sensing measurement of ZnO NRs to CO_2 gas.

Sa.	sensitivity			Response time (s)			Recovery time (s)		
	Gas concentration (ppm)			Gas concentration (ppm)			Gas concentration (ppm)		
	1000	2000	3000	1000	2000	3000	1000	2000	3000
t_1	30	10	30	67	56	47	33	26	36
t_2	35	12	36	65	53	45	32	24	51
t_3	52	15	55	67	55	39	31	36	52
t_4	60	15	70	65	53	37	28	36	52

The sensitivity to the CO_2 gas was calculated using Eq. (3). It increased significantly with increasing concentration of the gas and aspect ratio of ZnO NRs, showing the highest sensitivity of 70 at the target gas concentration of 3000 ppm for t_4 and aspect ratio of 4.9 compared to other samples with aspect ratios of less than 4. This increase leads to an increase in the absorption of gas molecules by ZnO NRs [37], particularly since this process was performed at a temperature of 50 ^{O}C. This resulted in a significant increase in sensitivity and a decrease in response time only at the gas concentration of 3000 ppm, while almost constant for other concentrations, as shown in Figure (8).

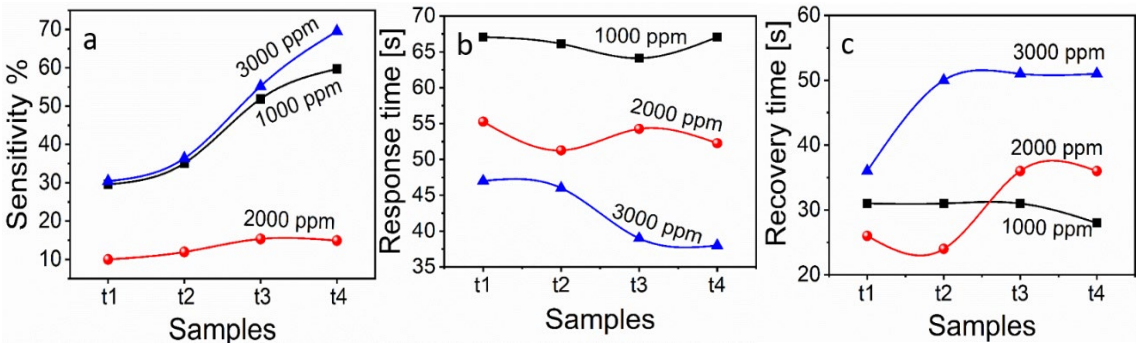

Fig. 8. ZnO NRs deposited on the glass substrate by RF sputtering for different CO_2 concentrations (a) Sensitivity, (b) Response time and (c) Recovery time.

The recovery time was increased with increasing aspect ratio of the ZnO NRs and gas concentration, other than 2000 ppm, which was almost constant due to saturation and relatively high operating temperature. Hence, the fabricated ZnO NRs demonstrated good sensitivity to NH_3 and CO_2 gases by comparing their response time to identical quantities of two gases.

4. Conclusion

In this study, ZnO NRs were grown on glass/ZnO seed layers with different thicknesses (1135, 1306, 1437, 1533 nm) by a hydrothermal method. The diffraction pattern for all models is polycrystalline with a wurtzite ZnO structure. The high aspect ratio of 4.9 for t_4 of ZnO NRs was achieved by varying ZnO seed layer thickness deposited by the RF sputtering method. Concerning NH_3 and CO_2 sensitivity, the response and recovery times increased with increasing aspect ratio of the ZnO NRs, which exhibit a gas response of 75.87 s and 65 s under exposure of 3000 ppm CO_2 and NH_3, respectively, at an operating temperature of 50 ^{O}C. This indicates that ZnO NRs with high aspect ratios could be effectively utilized as NH_3 and CO_2 sensors.

Acknowledgements

The authors would like to express their gratitude and acknowledge the department of physics staff at the college of science of the Mustansiriyah University, the Laboratory of Advanced Materials, for making the necessary measurements.

References

[1] S.-J. Young, Y.-L. Chu, IEEE Transactions on Electron Devices, vol. 68, no. 4, pp. 1886-1891, 2021; https://doi.org/10.1109/TED.2021.3060354

[2] M. Padvi, A. Moholkar, S. Prasad, N. Prasad, Engineered Science, vol. 15, pp. 20-37, 2021; https://doi.org/10.30919/es8d431

[3] Hassan ES, Abdulmunem OM, Brazilian Journal of Physics vol.52, no.5, pp.160, 2022; https://doi.org/10.1007/s13538-022-01158-9

[4] I.-D. Kim, A. Rothschild, H. L. Tuller, Acta Materialia, vol. 61, no. 3, pp. 974-1000, 2013; https://doi.org/10.1016/j.actamat.2012.10.041

[5] S. Das, V. Jayaraman, Progress in Materials Science, vol. 66, pp. 112-255, 2014; https://doi.org/10.1016/j.pmatsci.2014.06.003

[6] H. M. Mikhlif, M. O. Dawood, O. M. Abdulmunem, Mohanad K. Mejbel. Acta Physica Polonica, A. 140, no. 4, 2021; https://doi.org/10.12693/APhysPolA.140.320

[7] X. Chen et al., Nano-micro letters, vol. 14, pp. 1-15, 2022; https://doi.org/10.1007/s40820-021-00740-1

[8] P. M. Bulemo, J. Y. Cheong, ACS Applied Nano Materials, 2023; https://doi.org/10.1021/acsanm.2c04447

[9] D. Wang, D. Zhang, Q. Pan, T. Wang, F. Chen, Sensors and Actuators B: Chemical, vol. 371, p. 132481, 2022; https://doi.org/10.1016/j.snb.2022.132481

[10] G. S. Sarma, K. Muruganandam, K. S. M. Ponvel, M. S. Chavali, Sustainable Nanomaterials for Biomedical Engineering: Impacts, Challenges, and Future Prospects, p. 31, 2023; https://doi.org/10.1201/9781003333456-3

[11] D. Panda, T.-Y. Tseng, Journal of Materials Science, vol. 48, pp. 6849-6877, 2013; https://doi.org/10.1007/s10853-013-7541-0

[12] X. Jin et al., Chemical Engineering Journal Advances, vol. 4, p. 100034, 2020; https://doi.org/10.1016/j.ceja.2020.100034

[13] T. Li et al., Nanomaterials, vol. 12, no. 6, p. 982, 2022; https://doi.org/10.3390/nano12060982
[14] N. A. C. Lah, Surfaces and Interfaces, p. 102819, 2023; https://doi.org/10.1016/j.surfin.2023.102819
[15] O. M. Abdulmunem, M. J. Ali, E. S. Hassan, Optical Materials vol 109, pp. 110374, 2020; https://doi.org/10.1016/j.optmat.2020.110374
[16] S. Agarwal et al., Sensors and Actuators B: Chemical, vol. 292, pp. 24-31, 2019; https://doi.org/10.1016/j.snb.2019.04.083
[17] D. Yang et al., Journal of King Saud University-Science, vol. 33, no. 3, p. 101397, 2021; https://doi.org/10.1016/j.jksus.2021.101397
[18] F.-R. Juang, B.-Y. Chen, Solid-State Electronics, vol. 164, p. 107711, 2020; https://doi.org/10.1016/j.sse.2019.107711
[19] T. Holland, A.M. Abdul-Munaim, D.G. Watson and P. Sivakumar, Lubricants, vol. 7, no. 1, p.4, 2019. https://doi.org/10.3390/lubricants7010004
[20] S. A. Abbas, E. S. Hassan, O. M. Abdulmunem, Dig. J. Nanomater. Bios. 18, 793 - 803 (2023);https://doi.org/10.15251/DJNB.2023.183.793
[21] R. Ahmad, S. M. Majhi, X. Zhang, T. M. Swager, K. N. Salama, Advances in colloid and interface science, vol. 270, pp. 1-27, 2019; https://doi.org/10.1016/j.cis.2019.05.006
[22] P. Wang, T. Dong, C. Jia, P. Yang, " Sensors and Actuators B: Chemical, vol. 288, pp. 1-11, 2019; https://doi.org/10.1016/j.snb.2019.02.095
[23] J.-H. Kim, A. Mirzaei, H. W. Kim, P. Wu, S. S. Kim, Sensors and Actuators B: Chemical, vol. 293, pp. 210-223, 2019; https://doi.org/10.1016/j.snb.2019.04.113
[24] A. Dey, Materials science and Engineering: B, vol. 229, pp. 206-217, 2018; https://doi.org/10.1016/j.mseb.2017.12.036
[25] O. Carp, C. L. Huisman, A. Reller, Progress in solid state chemistry, vol. 32, no. 1-2, pp. 33-177, 2004; https://doi.org/10.1016/j.progsolidstchem.2004.08.001
[26] A. Wei, L. Pan, W. Huang, Materials Science and Engineering: B, vol. 176, no. 18, pp. 1409-1421, 2011; https://doi.org/10.1016/j.mseb.2011.09.005
[27] D. Zhang, C. Jiang, Journal of Alloys and Compounds, vol. 698, pp. 476-483, 2017; https://doi.org/10.1016/j.jallcom.2016.12.222
[28] T.-Y. Chen et al., Sensors and Actuators B: Chemical, vol. 221, pp. 491-498, 2015; https://doi.org/10.1016/j.snb.2015.06.122
[29] M. González-Garnica et al., Sensors and Actuators B: Chemical, vol. 337, p. 129765, 2021; https://doi.org/10.1016/j.snb.2021.129765
[30] Ehssan S. Hassan, Abdulhussain K. Elttayef, Suzan Hadi Mostafa, Mohammed Hadi Salim, Sami Salman Chiad, Journal of Materials Science: Materials in Electronics, Netherlands; https://doi.org/10.1007/s10854-019-01954-1
[31] J. M. Walker, S. A. Akbar, P. A. Morris, Sensors and Actuators B: Chemical, vol. 286, pp. 624-640, 2019; https://doi.org/10.1016/j.snb.2019.01.049
[32] Y. Kang, F. Yu, L. Zhang, W. Wang, L. Chen, Y. Li, Solid State Ionics, vol. 360, p. 115544, 2021; https://doi.org/10.1016/j.ssi.2020.115544
[33] Y. Huang et al., Nature communications, vol. 12, no. 1, p. 21, 2021; https://doi.org/10.1038/s41467-020-20209-w
[34] J. Huh, J. Park, G. T. Kim, J. Y. Park, Nanotechnology, vol. 22, no. 8, p. 085502, 2011; https://doi.org/10.1088/0957-4484/22/8/085502
[35] S. M. Majhi, A. Mirzaei, S. Navale, H. W. Kim, S. S. Kim, Nanoscale, vol. 13, no. 9, pp. 4728-4757, 2021; https://doi.org/10.1039/D0NR08448D
[36] N. Harale et al., Ceramics International, vol. 42, no. 11, pp. 12807-12814, 2016; https://doi.org/10.1016/j.ceramint.2016.05.044
[37] F. Sarf, Gas Sensors, vol. 1, 2020; https://doi.org/10.5772/intechopen.88858